Geophysical Research Letters

RESEARCH LETTER
10.1029/2020GL091467

Mesoscale Structures in Earth's Magnetotail Observed Using Energetic Neutral Atom Imaging

A. M. Keesee[1,2], N. Buzulukova[3,4], C. Mouikis[2], and E. E. Scime[5]

[1]Department of Physics and Astronomy, University of New Hampshire, Durham, NH, USA, [2]Space Science Center, University of New Hampshire, Durham, NH, USA, [3]Goddard Space Flight Center, Greenbelt, MD, USA, [4]University of Maryland, College Park, MD, USA, [5]Department of Physics and Astronomy, West Virginia University, Morgantown, WV, USA

Key Points:

- An interval of bursty flows during a magnetospheric substorm expansion phase is observed by Two Wide-angle Imaging Neutral-atom Spectrometers (TWINS), Magnetospheric MultiScale (MMS), and Active Magnetosphere and Planetary Electrodyamics Response Experiment and simulated using the Space Weather Modeling Framework
- The localized regions of ion heating observed by TWINS are directly related to the bursty plasma flow channel and substorm development
- The observed heating is less intense in the simulations than the TWINS and MMS data; additional heating processes are needed in the model

Correspondence to:

A. M. Keesee
amy.keesee@unh.edu

Citation:

Keesee, A. M., Buzulukova, N., Mouikis, C., & Scime, E. E. (2021). Mesoscale structures in Earth's magnetotail observed using energetic neutral atom imaging. *Geophysical Research Letters*, *48*, e2020GL091467. https://doi.org/10.1029/2020GL091467

Received 30 OCT 2020
Accepted 17 DEC 2020

Abstract Mesoscale structures in Earth's magnetotail are a primary feature of particle transport to the inner magnetosphere during storms and substorms. We demonstrate that such structures can be observed in energetic neutral atom (ENA) data which can provide remote, global images of the magnetosphere. In particular, we present localized regions of increased ion temperatures that appear in equatorial ion temperature maps calculated from Two Wide-angle Imaging Neutral-atom Spectrometers (TWINS) ENA data. These regions are associated with a dipolarization front with bursty ion flows measured by Magnetospheric MultiScale (MMS) and are concurrent with substorm features observed in field aligned currents (FAC) from Active Magnetosphere and Planetary Electrodynamics Response Experiment measurements. We conduct a magnetohydrodynamics simulation of the same event and show simulated ion temperatures, ion flows, and FACs that agree with the measurements. However, the observed plasma heating is less intense in the simulated results than in the TWINS and MMS data, indicating that some heating processes may be missing from the model.

Plain Language Summary Large chunks of energetic particles and enhanced magnetic field from the Sun can cause geomagnetic storms and substorms in the space surrounding Earth. During these active times, the energy from the Sun can get dumped into the nightside where ions and electrons are heated and propelled toward the Earth like from a slingshot. When these energetic particles get closer to the Earth, they can disrupt satellites and cause power outages, so scientists hope to improve our understanding and develop forecasting tools for these storms and substorms. Scientists have shown that the particles move toward the Earth in narrow channels. We demonstrate that these channels are heated and can be seen in temperature maps created from the NASA TWINS mission. To support our findings, we also compare the results to measurements from other satellites and computer simulations. This means that we can use such maps for more research and to improve forecasting models. For example, we found that the measured temperatures are higher than the simulated temperatures, indicating that more is needed in the models. We could also use a satellite like TWINS to act as a warning system for storms and substorms.

1. Introduction

Plasma from Earth's magnetotail is transported earthward during storms and substorms, driving the dynamics in the inner magnetosphere. Rather than forming a continuous flow across the entire magnetotail, it has been found that the particles are transported in a localized, bursty way (Angelopoulos et al., 1992). Studies have shown that there is a dusk-ward preference for these flows (Gabrielse et al., 2014) that result in injections to the inner magnetosphere. The particles appear to be transported in narrow flow channels of ~2–3 R_E, measured with in situ instruments (Nakamura et al., 2004). In magnetohydrodynamics (MHD) simulations, the channels are ~1−2 R_E, but the width of these channels tends to be dependent on the simulation grid resolution (Wiltberger et al., 2015). It has been unclear whether such narrow features could be imaged remotely by energetic neutral atom (ENA) instruments. If this is possible, an ENA imager could be used as a space weather monitor to provide warnings of potential threats to satellites, communications systems, and the power grid. C:son Brandt et al. (2002) reported observations of narrow flow channel features using a parameterized model of the ring current to extract the ion distribution from ENA images from the Astrid-1 microsatellite. While one such observation occurred around the time of a substorm injection,

the same feature was observed 24 h earlier with no evidence of an injection. Thus, it is unclear if this was evidence of storm or substorm dynamics. Keesee et al. (2014) observed regions of enhanced ion temperatures calculated from ENA data during the intense storm-time substorm associated with the loss of the Galaxy-15 satellite. The regions initially appeared beyond 10 R_E and were deflected dawnward just outside of geosynchronous orbit. This was an especially intense interval, so understanding the ability for ENA instruments to make similar observations during other levels of activity is needed. In this study, we present evidence that ENA images can be used to observe narrow features of particle injections during a moderate storm. We show that during an interval in which regions of enhanced ion temperatures are observed in the temperature maps calculated from Two Wide-angle Imaging Neutral Spectrometers (TWINS) ENA data, in situ Magnetospheric MultiScale (MMS) measurements from the same location indicate the arrival of a dipolarization front. In addition, simultaneous Active Magnetosphere and Planetary Electrodynamics Response Experiment (AMPERE) measurements demonstrate the presence of a field aligned current structure consistent with substorm activity. We also conduct global MHD simulations of the interval and compare the output with the TWINS, MMS, and AMPERE observations.

2. Methodology

2.1. TWINS Ion Temperature Maps

The 2D plasma sheet ion temperature maps are calculated using ENA data from the NASA Two Wide-angle Imaging Neutral Spectrometers (TWINS) mission (McComas et al., 2009). For this study, 2-sweep (approximately 3 min) averages of ENA flux in 13 energy bins from 2–32 keV are projected along the instrument line of sight to a 0.5×0.5 R_E grid in the equatorial plane in geocentric solar magnetospheric (GSM) coordinates. Within each grid bin, a fit to the ENA spectrum for a Maxwellian parent ion distribution is used to calculate an ion temperature. The region within 3 R_E of the Earth is excluded because low altitude ENA emissions violate assumptions of the fitting method (Bazell et al., 2010) and bins outside a modeled magnetosphere boundary using Shue et al. (1997) are ignored. More details on the calculation and validation of the ion temperature maps are described by Keesee et al. (2014) and Keesee et al. (2020), while the software used is available at Keesee et al. (2019).

2.2. MMS and AMPERE Supporting Data

Data from the Hot Plasma Composition Analyzer (HPCA) and Fluxgate Magnetometer (FGM) instruments on the NASA Magnetospheric MultiScale (MMS) mission (Burch et al., 2016) are used to obtain in situ proton and magnetic field measurements. The interval reported in this study is during the MMS Phase 1x when the apogee was at 12 R_E on the nightside (Fuselier et al., 2015).

Field aligned current density measurements are obtained from the Active Magnetosphere and Planetary Electrodynamics Response Experiment (AMPERE) summary plots available at the AMPERE Data Center. These plots are 10-min averages available every 2 min.

2.3. Global MHD BATS-R-US Simulations

To study the global magnetospheric dynamics during this interval, we perform simulations using the global BATS-R-US magnetohydrodyamics (MHD) model (Tóth et al., 2005, 2012). The global MHD model is coupled in a two-way mode with the ionospheric solver in the Space Weather Modeling Framework (SWMF). In this particular setup, we use the ideal isotropic version of BATS-R-US MHD with grid resolution 1/8 R_E in the near-Earth region. The total number of grid points is $\sim 12 \times 10^6$. The ionospheric conductivity is calculated from an empirical relation between field-aligned currents and ionospheric conductivity specified with the Assimilative Mapping of Ionospheric Electrodynamics (AMIE) model (Ridley et al., 2004).

The ionospheric solver output includes field-aligned currents, therefore presenting an opportunity to compare the model results with the AMPERE observations. In addition, a proxy for the ionospheric indices AU/AL/AE is calculated from the simulations. For this purpose, the variations of the magnetic field are output at the surface of the Earth at 36 ground-based stations located between 65 and 75° of magnetic latitude (12 points in magnetic longitude, 3 points in magnetic latitude). Lower/upper envelopes of dB variations for the

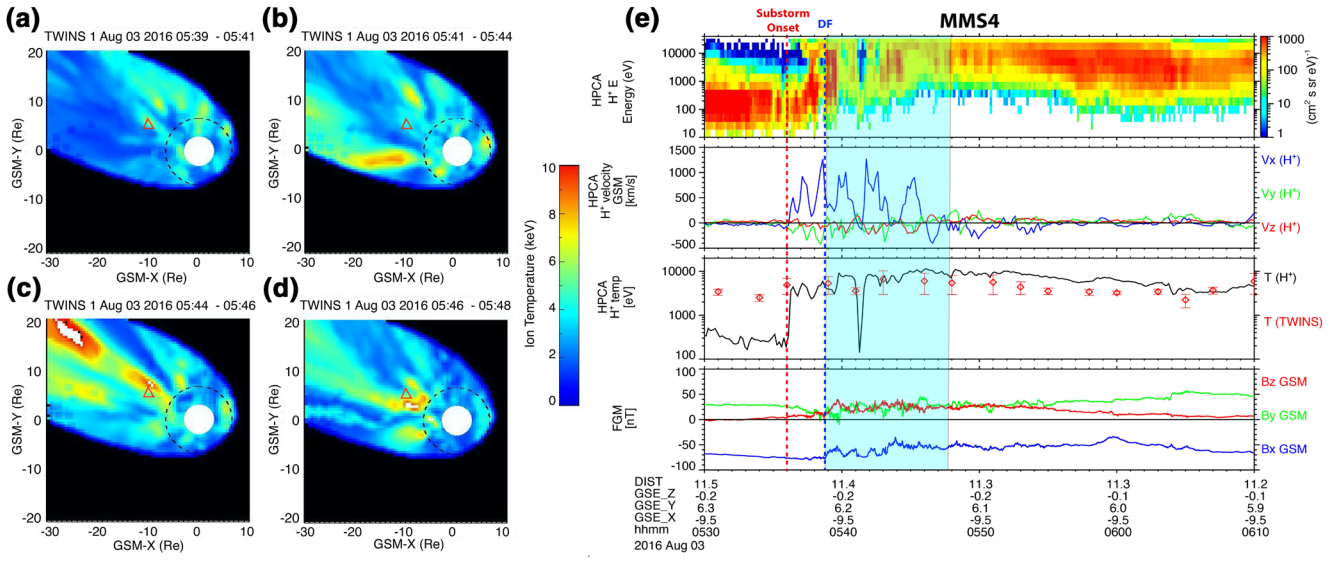

Figure 1. (a–d) Two Wide-Angle Imaging Neutral-Atom Spectrometers (TWINS) ion temperature maps with a 2 min time cadence for 3 August 2016, 5:39–5:48 UT. The Sun is to the right. The white disk has a radius of 3 R_E and is centered at Earth. The dashed line indicates geosynchronous orbit and the triangle designates the *x*,*y* coordinates of MMS4. (e) Measurements from the MMS4 satellite from top to bottom: proton flux spectrogram, proton velocity components, proton temperature, and magnetic field components. On the third panel, red crosses indicate the temperature from the TWINS map at the *x*,*y* location of MMS4. The shaded region indicates the interval covered by (a–d). The vertical red line indicates substorm onset and the vertical blue line indicates a dipolarization in the magnetic field measurements.

northward component (H-component) of the magnetic field are calculated as a proxy for synthetic AU and AL indices, with the difference between these indices giving the AE index. Comparison of the simulated field-aligned currents and synthetic indices with the observed AMPERE data and AU, AL, and AE indices will allow for identifying the corresponding time intervals that will be used to identify which time intervals in the simulation correspond to the which real time intervals for comparison to the MMS and TWINS data.

3. Results

TWINS ion temperature maps for 3 August 2016, 5:39–5:48 UT are shown in Figure 1 along with the in situ measurements from the MMS4 satellite for the interval 5:30–6:20 UT. This interval coincides with the beginning of the main phase of a moderate storm (min Dst = -52 nT). In addition, a substorm onset has been identified at 5:36 UT (marked by red dashed line in Figure 1e) according to the SuperMAG substorm onset database (Gjerloev, 2012). Multiple regions of enhanced ion temperatures are observed during this period across the tail in the TWINS maps. One such region appears on the dawn side of the tail beginning at 5:41–5:44 UT (Figure 1b), and is deflected toward the dawn flank near geosynchronous orbit (Figures 1c and 1d). Another region of enhanced localized ion temperatures develops on the dusk side of the tail near the location of the MMS satellites (shown as a triangle in the TWINS images). The peak temperature in this region is $T_i \sim 5$ keV at 5:39 UT (Figure 1a) and increases to >10 keV at 5:44 UT (Figure 1c). During this interval MMS4 (Figure 1e) observes increased ion energies (top panel), Earthward flow bursts (V_x) followed by an interval of tailward flows (second panel), increased ion temperatures, and a dipolarization (indicated by the blue dashed vertical line) of B_z. The red crosses indicate the calculated temperature from the TWINS data at the MMS position in the *x*,*y* GSM plane. Right before the substorm onset, the calculated TWINS temperatures differ from the MMS observed ion temperatures because MMS was in the lobe due to current sheet thinning during the substorm growth phase. After the substorm onset, the agreement between TWINS and MMS plasma sheet ion temperatures is remarkable.

The interval from August 02, 20 UT to August 03, 06 UT was simulated using the BATS-R-US MHD model. The IMF B_z, Kyoto AU and AL auroral indices, and synthetic AU and AL indices are shown in Figure 2. A vertical black dashed line marks the southward B_z turning around 4:35 UT. Due to the numerical effects and imperfect propagation of solar wind data to the MHD boundary at $x = 30$ R_E, the global code reproduces

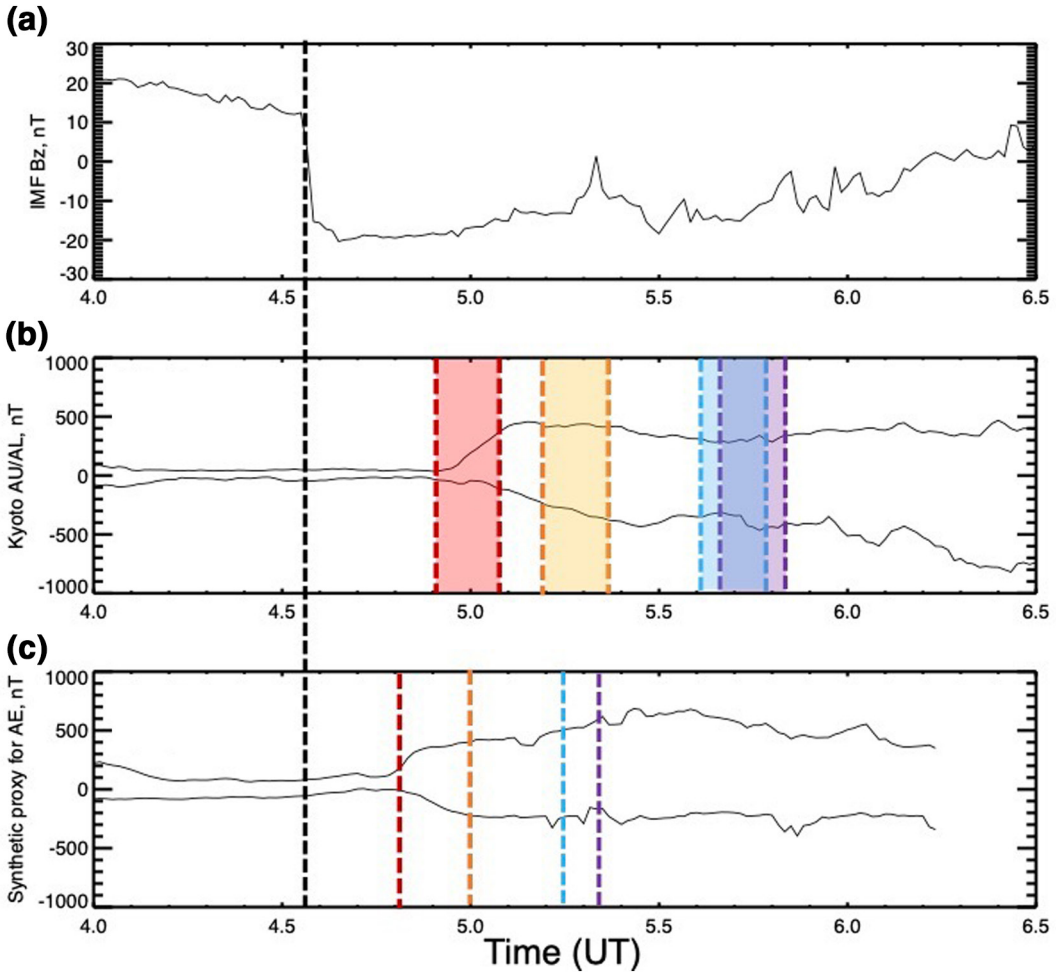

Figure 2. (a) OMNI 1-min solar wind Bz for 3 August 2016, 04:00-06:30 UT, shifted to X = 30 R_E. (b) Kyoto auroral indices AU and AL; (c) Modeled synthetic auroral indices AU and AL. Black dashed line shows the northward-southward Bz turning. Four intervals are selected for data-model comparison between AMPERE and BATS-R-US ionospheric solver: (i) 04:54–05:04 UT, red rectangular area; (ii) 05:12–05:22 UT, yellow rectangular area; (iii) 05:36–05:46 UT, blue rectangular area; (iv) 05:38–05:48 UT, violet rectangular area. Corresponding time snapshots in the model are chosen to be 04:50 UT, 05:50 UT, 05:15 UT, 05:20 UT, see the text for the details.

the observed phenomena with slightly different timing. The details of the timing are reconstructed from the comparison between auroral indices and AMPERE data with the corresponding model proxies. For the purposes of comparison between 10 min averages of AMPERE data and the simultaneous model output, the selected intervals are outlined by color shadowing in Figure 2b; the corresponding simultaneous time snapshots are shown by color dashed lines in Figure 2c.

The southward IMF arrives at the bowshock ~24 min after the Bz turning shown in Figure 2a. This is demonstrated by the onset of auroral activity (red lines in Figure 2b). A shorter arrival time of ~15 min is observed in the simulation, indicated by onset of auroral activity at the red line in Figure 2c. The AU index began increasing and AL began decreasing, indicating quick development of an enhanced convection (yellow shaded area and yellow dashed lines in Figures 2b and 2c). The last interval 05:36–05:46 UT (violet dashed lines in Figure 2b) is the interval when MMS s/c see the bursty bulk flow, and TWINS observes the channel of enhanced temperature. The corresponding time snapshot from the model is deduced to be at ~05:20 UT. The choice of this particular model time snapshot is justified from the comparison with AMPERE data (see below). The interval a few minutes before the flow onset is also selected for comparison (blue dashed lines in Figures 2b and 2c).

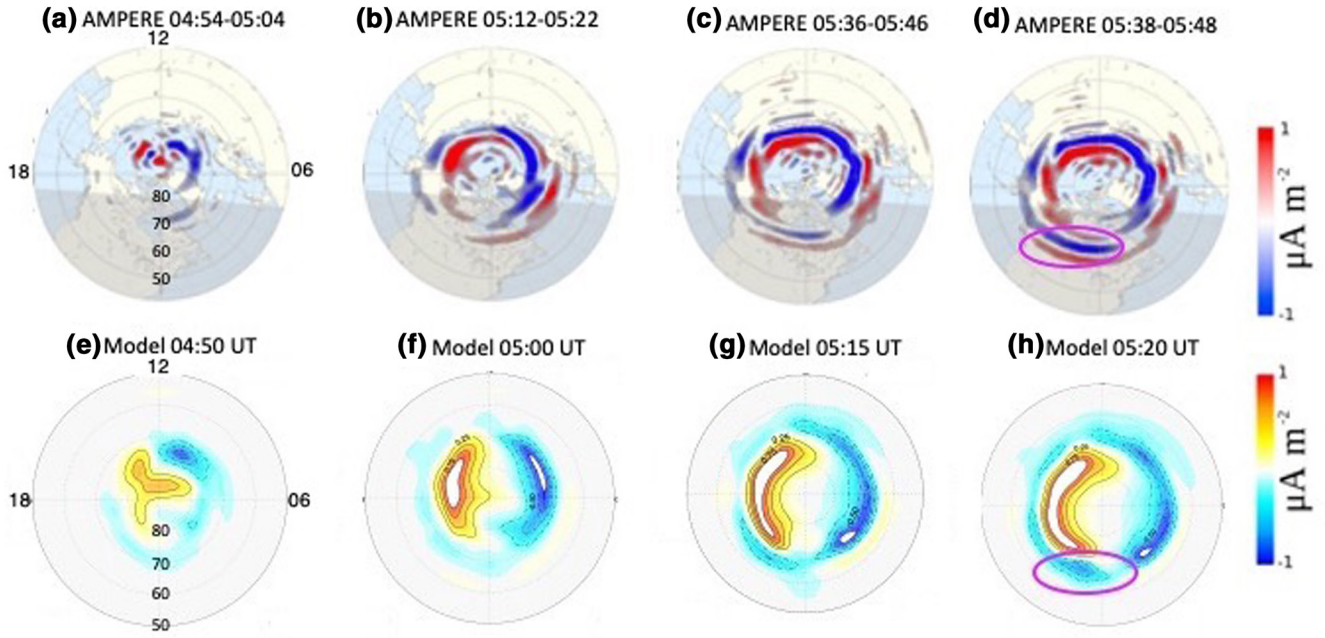

Figure 3. (a–d) AMPERE field-aligned currents for four intervals from Figure 2. Noon MLT is on top. Upward currents are in red and downward in blue. (e–h) Model results for field-aligned currents from BATS-R-US ionospheric solver. The latitude for each is indicated in panels (a) and (e). The magenta oval on panel (d) marks an area of enhanced field-aligned currents associated with substorm development and formation of the bursty flow observed by MMS. The magenta oval in the panel (h) shows the corresponding structure in the modeled field-aligned currents.

The evolution of the field aligned current (FAC) pattern using data from AMPERE is shown in Figures 3a–3d, with the intervals selected shown in 2b. At 4:54–5:04 UT a typical quiet pattern is observed (Figure 3a), just before the propagation of the disturbance associated with southward Bz ('red' interval in Figure 2). At 5:12–5:22 UT (Figure 3b) a 2-cell pattern indicative of magnetosphere convection has developed ('yellow' interval in Figure 2). At 5:36–5:46 UT (Figure 3c) an additional current structure can be seen beginning to develop in the premidnight sector ('blue' interval in Figure 2). In the interval beginning 2 minutes later (Figure 3d) this feature is fully developed, indicated by the magenta oval ('violet' interval in Figure 2). This layered structure of FACs shown in the magenta oval has been shown to be consistent with the classical substorm current wedge (SCW) structure and is often present during the substorm expansion phase (Murphy et al., 2013).

The simulated FAC using the BATS-R-US ionospheric solver are shown in Figures 3e–3h for the intervals indicated in Figure 2c. As noted previously, the times are not exact as in the observations, but the pattern is similar. In the fourth interval (Figure 3h), the substorm-like structure in the premidnight sector also appears in the simulations (indicated by magnenta oval). As noted in Buzulukova et al. (2018), the layered structure of FACs during the substorm expansion phase resembles the Harang discontinuity structure reported in global Hall simulations of the 'mini-Earth' Ganymede (Dorelli et al., 2015). The modeled structure has maximum intensity during 05:20–05:25 UT, thus justifying the choice of time snapshot 05:20 UT to be compared with TWINS temperature maps.

Figure 4 shows the simulated isovolumes of ion (plasma) temperature (polar and side views; panels a and b) and x-component of the bulk plasma velocity, U_x, (panel c) at 5:20 UT. A region of enhanced ion temperatures and enhanced earthward flow is observed in the premidnight sector, very close to the location of MMS s/c (yellow sphere in Figure 4). Based on the FAC pattern in Figures 3d and 3h, 5:20 UT in the simulation corresponds to 5:38–5:48 UT in real time, and particularly the latter portion of that interval since the substorm feature in ionospheric FACs is less prominent in the 2-min earlier AMPERE average in Figure 3c. Thus, these simulation plots can be compared to the TWINS ion temperature maps in Figures 1c and 1d. The two-part structure seen in Figure 1c (one region of enhanced ion temperatures centered around $x = -10\ R_E$ and one extending $x = -20$ to $-30\ R_E$) corresponds to the two-part structure observed in the

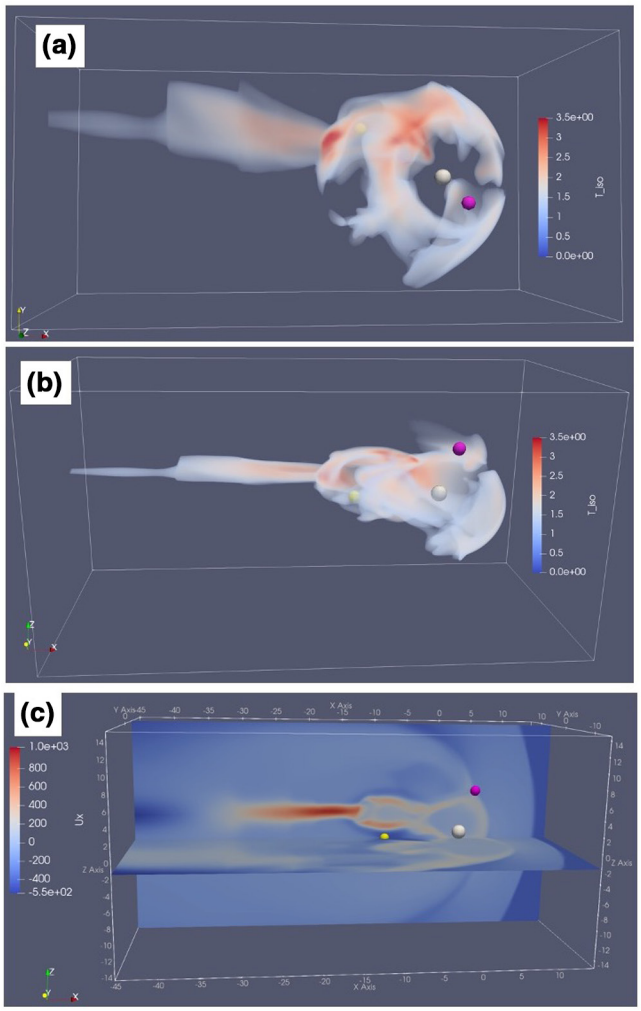

Figure 4. BATS-R-US model results at 05:20 UT for the simulation domain X = [-45,15]; Y = [-15,15]; Z = [-15; 15] R_E. (a) Isovolume of temperature, in keV, polar view; (b) Isovolume of temperature, in keV, side view; (c) 2D plane cuts through MMS location, XYZ (GSM) = [-10,6,-2] R_E with U_X component of bulk plasma velocity, km/sec. Magenta and yellow spheres mark location of TWINS1 and MMS s/c at 05:20 UT and the white sphere is Earth.

simulations with an enhanced region that extends from $x = -15$ to -30 R_E and one closer to the Earth that spreads out in the z-direction. Also, the spatial structure seen in Figure 1d is similar to that in Figure 4a. The region of an enhanced U_x component is embedded into the region of an enhanced plasma temperature, thus confirming the MMS and TWINS do likely see the same structure.

The two-dimensional (2D) plane cut of the x-component of bulk plasma velocity shows a reversal in U_x located in the tail at ~35 R_E, thus indicating a possible X-line and reconnection location. A detailed analysis of the structure and dynamics of the X-line for this event is beyond the scope of the present paper and will be done elsewhere.

4. Discussion and Summary

For the first time, we demonstrate the relationship between local observations of the plasma heating observed in the bursty bulk flow by MMS s/c and global observations of a channel of plasma heating in the tail detected by TWINS ENA imagers. We interpret the observations of the development of an intense bursty flow during the magnetospheric substorm expansion phase, as supported by AMPERE data analysis and MHD model results. The model suggests that the plasma heating observed by TWINS is directly related to the development of the bursty plasma flow and the substorm development. The model results also suggest that the development of an intense bursty flow in the model is related to the reconnection and X-line located at ~35 R_E. The bursty flows in the model deaccelerate in the near-Earth region, thus creating a characteristic structure in FACs. The layered structure in FACs seen by AMPERE is reported to appear during the substorm expansion phase, and is consistent with a SCW model (Murphy et al., 2013). The observations of MMS, TWINS, and AMPERE therefore are connected and supported by global simulations.

What controls the temperature increase in the MHD model? In ideal MHD, the only process that changes the internal energy of the fluid is the compression effects (Schindler, 2006). In terms of individual particle motion, this could be interpreted as heating due to conservation of adiabatic invariants when the particles in the bursty flow move from the stretched field lines in the tail to the dipole-like region near the Earth. The observed plasma heating is less intense in the MHD results than in the TWINS and MMS data. This is likely because the ideal MHD misses many important aspects of the local physics, including kinetic effects and wave-particle interactions. However, the model predicts the global structure of the heated region, and also allows the connection of multiple measurements with a cause-effect relationship. The community currently debates about the contribution of different processes to the particle energization in the bursty flows and in the near-Earth region. Hybrid simulations by Lin et al. (2014) demonstrate that ion heating is due to wave-particle and ion-pickup interactions. Birn et al. (2017) and Zhou et al. (2018) used test particle simulations to show that ions experience betatron acceleration when entering dipolarizing flux bundle regions with enhanced electric fields. Gabrielse et al. (2019) recently used observations from multiple ground- and satellite-based instruments to demonstrate that the varying size and location of particle energization events observed in previous studies are actually different parts of the same phenomenon. It is very important that ENA measurements can provide a quantitative global picture of plasma heating, and thus contribute to this work to constrain the models and theories. The TWINS data can be used in conjunction with in situ measurements from MMS, THEMIS, AMPERE, and other missions for further study of these phenomena.

We have demonstrated that it is possible to observe narrow structures in ENA data that are evidence of flow channels resulting from magnetic reconnection in Earth's magnetotail. Combined with data from other

missions and instruments, ENA maps provide a powerful method to track global energy flows in near Earth space. This and similar studies will be helpful for designing future space weather dedicated missions, including the Solar-Terrestrial Observer for the Response of the Magnetosphere (STORM) mission recently selected by NASA for Phase A study. An ENA imager could also be considered for a space weather monitor. To get an idea for the lead time necessary for such an application, we can consider that Baker et al. (2016) observed particle injections from the tail with MMS to the inner magnetosphere with the Van Allen Probes and found the electrons within a dipolarization front traveled from $-10\ R_E$ to $-4.5\ R_E$ in approximately 6 min. Proton ENAs with an energy of 10 keV traveling from a source location at $x = -10\ R_E$ to a monitor at the TWINS1 location during this interval of $(x, y, z) = (1, -3, 6)\ R_E$ would take about a minute, providing some lead time to the actual injection of particles in the inner magnetosphere if the data can be analyzed and downlinked quickly.

Data Availability Statement

TWINS data are available on CDAWeb (https://cdaweb.gsfc.nasa.gov/index.html/). A database of storm-time ion temperatures using the method described at 10-min time cadence is also available on CDAWeb. The projected TWINS ENA flux and calculated ion temperatures used for Figures 1a–1d have been made available online for download at https://doi.org/10.5281/zenodo.4338742. AMPERE summary plots were obtained at http://ampere.jhuapl.edu/products/plots/index.html. The BATS-R-US global MHD model and ionospheric solver are parts of SWMF code and were developed by the Center for Space Environment Modeling at the University of Michigan. Resources supporting this work were provided by the NASA High-End Computing (HEC) Program through the NASA Advanced Supercomputing (NAS) Division at Ames Research Center. The model output data used in production of Figures 2–4 have been made available online for download at http://doi.org/10.5281/zenodo.4318149 .

Acknowledgments
The authors thank the TWINS science team for fruitful discussions in the development of the ENA analysis and ion temperature calculation technique. The authors thank the AMPERE team and the AMPERE Science Center for providing the Iridium-derived data products. The authors thank the MMS team, especially the HPCA and FGM instrument teams, for providing the MMS data products, which are available at https://lasp.colorado.edu/mms/sdc/public/.

References

Angelopoulos, V., Kennel, C. F., Kivelson, M. G., Walker, R. J., & Paschmann, G. (1992). Bursty bulk flows in the inner central plasma sheet. *Journal of Geophysical Research*, *97*(A4), 4027–4039.

Baker, D. N., Jaynes, A. N., Turner, D. L., Nakamura, R., Schmid, D., Mauk, B. H., & Burch, J. L. (2016). A telescopic and microscopic examination of acceleration in the June 2015 geomagnetic storm: Magnetospheric multiscale and Van Allen Probes study of substorm particle injection. *Geophysical Research Letters*, *43*(12), 6051–6059. https://doi.org/10.1002/2016GL069643

Bazell, D., Roelof, E. C., Sotirelis, T., Brandt, P. C., Nair, H., Valek, P., McComas, D. (2010). Comparison of TWINS images of low-altitude emission of energetic neutral atoms with DMSP precipitating ion fluxes. *Journal of Geophysical Research*, *115*(A10), 1–17. Retrieved from http://www.agu.org/pubs/crossref/2010/2010JA015644.shtml; https://doi.org/10.1029/2010JA015644

Birn, J., Runov, A., & Zhou, X. Z. (2017). Ion velocity distributions in dipolarization events: Distributions in the central plasma sheet. *Journal of Geophysical Research: Space Physics*, *123*, 429–442. https://doi.org/10.1002/2017JA024230

Burch, J. L., Moore, T. E., Torbert, R. B., & Giles, B. L. (2016). Magnetospheric Multiscale Overview and Science Objectives. *Space Science Reviews*, *199*(1–4), 5–21. Retrieved from http://dx.doi.org/10.1007/s11214-015-0164-9; https://doi.org/10.1007/s11214-015-0164-9

Buzulukova, N., Goldstein, J., Fok, M. C., Glocer, A., Valek, P., McComas, D., & Anderson, B. (2018). Magnetosphere dynamics during the 14 November 2012 storm inferred from TWINS, AMPERE, Van Allen Probes, and BATS-R-US-CRCM. *Annales Geophysicae*, *36*(1), 107–124. https://doi.org/10.5194/angeo-36-107-2018

C:son Brandt, P., Ebihara, Y., Barabash, S., & Roelof, E. C. (2002). Energetic neutral atom images of a narrow flow channel from the plasma sheet: Astrid-1 observations. *Journal of Geophysical Research*, *107*(A10), 1–8. Retrieved from http://www.agu.org/pubs/crossref/2002/2001JA000230.shtml; https://doi.org/10.1029/2001JA000230

Dorelli, J. C., Glocer, A., Collinson, G., & Tóth, G. (2015). The role of the Hall effect in the global structure and dynamics of planetary magnetospheres: Ganymede as a case study. *Journal of Geophysical Research: Space Physics*, *120*(7), 5377–5392. https://doi.org/10.1002/2014JA020951

Fuselier, S. A., Dayeh, M. A., Livadiotis, G., McComas, D. J., Ogasawara, K., Valek, P., & Petrinec, S. M. (2015). Imaging the development of the cold dense plasma sheet. *Geophysical Research Letters*, *42*(19), 7867–7873. https://doi.org/10.1002/2015GL065716

Gabrielse, C., Angelopoulos, V., Runov, A., & Turner, D. L. (2014). Statistical characteristics of particle injections throughout the equatorial magnetotail. *Journal of Geophysical Research: Space Physics*, *119*, 2512–2535. Retrieved from http://onlinelibrary.wiley.com/doi/10.1002/2013JA019638/full; https://doi.org/10.1002/2013JA019638

Gabrielse, C., Spanswick, E., Artemyev, A., Nishimura, Y., Runov, A., Lyons, L., & Donovan, E. (2019). Utilizing the heliophysics/geospace system observatory to understand particle injections: their scale sizes and propagation directions. *Journal of Geophysical Research: Space Physics*, *119*, 5584–5609. https://doi.org/10.1029/2018ja025588

Gjerloev, J. W. (2012). The SuperMAG data processing technique. *Journal of Geophysical Research: Space Physics*, *117*(9), 1–19. https://doi.org/10.1029/2012JA017683

Keesee, A., Chen, M. W., Scime, E. E., & Lui, A. T. Y. (2014). Regions of ion energization observed during the Galaxy-15 substorm with TWINS. *Journal of Geophysical Research: Space Physics*, *119*, 8274–8287. https://doi.org/10.1002/2014JA020466

Keesee, A., Katus, R. M., Floyd, M., & Scime, E. (2020). Database of storm-time equatorial ion temperatures in Earth's magnetosphere calculated from energetic neutral atom data. *Journal of Geophysical Research: Space Physics*, *125*, 1–9. https://doi.org/10.1029/2020JA028266

Keesee, A., Scime, E., Zaniewski, A., & Katus, R. (2019). 2D ion temperature maps from TWINS ENA data: IDL scripts. *UNH Scholars' Repository*. https://doi.org/10.34051/c/2019.1

Lin, Y., Wang, X. Y., Lu, S., Perez, J. D., & Lu, Q. (2014). Investigation of storm time magnetotail and ion injection using three-dimensional global hybrid simulation. *Journal of Geophysical Research: Space Physics*, *119*(9), 7413–7432. Retrieved from http://onlinelibrary.wiley.com/doi/10.1002/2014JA020005/full; https://doi.org/10.1002/2014JA020005

McComas, D. J., Allegrini, F., Baldonado, J., Blake, B., Brandt, P. C., Burch, J., & Zoennchen, J. (2009). The Two Wide-angle Imaging Neutral-atom Spectrometers (TWINS) NASA mission-of-opportunity. *Space Science Reviews*, *142*(1–4), 157–231. Retrieved from http://www.springerlink.com/index/10.1007/s11214-008-9467-4; https://doi.org/10.1007/s11214-008-9467-4

Murphy, K. R., Mann, I. R., Rae, I. J., Waters, C. L., Frey, H. U., Kale, A., & Korth, H. (2013). The detailed spatial structure of field-aligned currents comprising the substorm current wedge. *Journal of Geophysical Research: Space Physics*, *118*(12), 7714–7727. https://doi.org/10.1002/2013JA018979

Nakamura, R., Baumjohann, W., Mouikis, C., Kistler, L. M., Runov, A., Volwerk, M., & Balogh, A. (2004). Spatial scale of high-speed flows in the plasma sheet observed by cluster. *Geophysical Research Letters*, *31*(9), L09804. Retrieved from http://doi.wiley.com/10.1029/2004GL019558; https://doi.org/10.1029/2004GL019558

Ridley, A. J., Gombosi, T. I., & DeZeeuw, D. L. (2004). Ionospheric control of the magnetosphere: Conductance. *Annales Geophysicae*, *22*(2), 567–584. https://doi.org/10.5194/angeo-22-567-2004

Schindler, K. (2006). *Physics of space plasma activity*. Cambridge University Press.

Shue, J.-H., Chao, J. K., Fu, H. C., Russell, C. T., Song, P., Khurana, K. K., & Singer, H. J. (1997). A new functional form to study the solar wind control of the magnetopause size and shape. *Journal of Geophysical Research*, *102*(A5), 9497. Retrieved from http://www.agu.org/pubs/crossref/1997/97JA00196.shtml; https://doi.org/10.1029/97JA00196

Tóth, G., Sokolov, I. V., Gombosi, T. I., Chesney, D. R., Clauer, C. R., De Zeeuw, D. L., et al. (2005). Space weather modeling framework: A new tool for the space science community. *Journal of Geophysical Research*, *110*(A12), A12226. Retrieved from http://doi.wiley.com/10.1029/2005JA011126; https://doi.org/10.1029/2005JA011126

Tóth, G., van der Holst, B., Sokolov, I. V., De Zeeuw, D. L., Gombosi, T. I., Fang, F., & Opher, M. (2012). Adaptive numerical algorithms in space weather modeling. *Journal of Computational Physics*, *231*(3), 870–903. https://doi.org/10.1016/j.jcp.2011.02.006

Wiltberger, M., Merkin, V., Lyon, J. G., & Ohtani, S. (2015). High-resolution global magnetohydrodynamic simulation of bursty bulk flows. *Journal of Geophysical Research: Space Physics*, *120*, 4555–4566. Retrieved from http://linkinghub.elsevier.com/retrieve/pii/S002199911100088X; https://doi.org/10.1002/2015JA021080

Zhou, X. Z., Runov, A., Angelopoulos, V., Artemyev, A. V., & Birn, J. (2018). On the acceleration and anisotropy of ions within magnetotail dipolarizing flux bundles. *Journal of Geophysical Research: Space Physics*, *122*, 1590–1599. https://doi.org/10.1002/2017JA024901